2nd URSI AT-RASC, Gran Canaria, 28 May – 1 June 2018

Dual-frequency Motion Compensation for SISAR Imaging in Forward Scatter Radar

Feifeng Liu(1), Changjiang Liu(1), Rui Wang* (1), and Cheng Hu (1) (2)
(1) School of Information and Electronics, Beijing Institute of Technology, Beijing, China
(2) Beijing Key Laboratory of Embedded Real-time Information Processing Technology, Beijing, China
*Email: bit.wangrui@gmail.com

Abstract

To solve the problem of motion compensation for accurate shadow inverse synthetic aperture radar (SISAR) imaging, an SISAR motion compensation algorithm based on dual-frequency is proposed. By conjugate multiplication of two echo signals with different carrier frequencies and different sampling rates, the influence of the scattering phase can be compensated and Doppler phase shift can be obtained by resolving recursive equations. Further, the Doppler variation rate at the baseline-crossing time is used as the initial value to solve the recursive equations. The simulation results show that this algorithm can give a more accurate SISAR contour image, the resolution of which has been greatly improved compared to that obtained by traditional SISAR motion compensation methods.

1. Introduction

As a kind of bistatic radar of special topology, forward scatter radar employs the enhancement of radar cross section (RCS) in forward scatter region and has great advantages in detecting stealth targets and low-slow-small targets compared with traditional monostatic radar [1]. Moreover, if applying the shadow inverse synthetic aperture radar (SISAR) imaging theory, it can extract target shadow profiles for recognition [2]. SISAR imaging technology utilizes the variation law of the target diffraction signal over time, and combines with the estimation of the target motion parameters to obtain the complex profile function (CPF) that contains the target silhouette information by inverse transforming the echo signal. Further, the target's two-dimensional silhouette contour features can be extracted from the CPF for target recognition and classification. In summary, SISAR imaging technology can provide with the length of the target, the silhouette contour, and other important features, being of great significance to the target recognition in forward scatter radar.

According to the applicable size of diffraction angle, the existing SISAR imaging methods are mainly divided into two kinds: small-diffraction-angle SISAR imaging and large-diffraction-angle SISAR imaging. Small-diffraction-angle SISAR imaging uses the traditional Fresnel diffraction integral based on the second-order approximation of the baseline slant range. Though the limited imaging resolution, the implementation of this SISAR imaging algorithm is simple and can be quickly calculated by fast Fourier transform (FFT). Moreover, the motion compensation needs only to estimate Doppler frequency variation rate [3]. For the large-diffraction-angle SISAR imaging, its signal model is improved based on the small-diffraction-angle SISAR imaging theory and the slant range modeling is acquired using the second-order expansion based on the target center-point slant range [4]. Thus a higher resolution can theoretically be obtained. However, its precondition is the accurate estimation of the target Doppler phase shift (or slope range) for motion compensation. As is known, the accuracy of the traditional tracking algorithm for slope range estimation is far from meeting the requirements of motion compensation. Therefore, the large-diffraction-angle SISAR imaging algorithm is now actually only a theoretical possibility.

To solve the problem of motion compensation for accurate SISAR imaging, we proposed an SISAR motion compensation method based on dual-frequency signal processing in this paper. Through the processing of different carrier frequency echoes, we can obtain the accurate estimation of the target slant range history, which is to be used in the motion compensation of SISAR imaging. The following sections are organized as follows. In Section 2, the basic principle for large-diffraction-angle SISAR imaging is introduced. In Section 3, the dual-frequency motion compensation method is proposed. In Section 4, simulation results are provided for discussion. Our conclusions are given in Section 5.

2. Large-diffraction-angle SISAR imaging

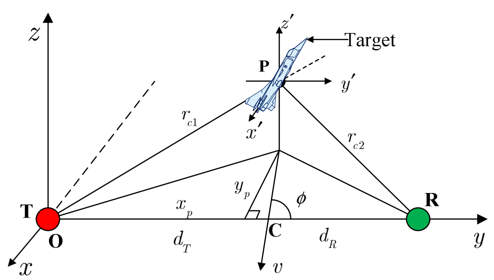

Figure 1. Forward scatter radar system topology.

The system topology used for shadow field modelling is shown in Fig. 1. The receiver locates in the origin of a Cartesian coordinate system (x, y, z), and the transmitter's position in this coordinate system is $(L, 0, 0)$, in which L is the length of the baseline. The local coordinate system (x', y', z'), the origin of which (x_p, y_p, z_p) is the target's center $\mathbf{P}$, is parallel to the global coordinate system (x, y, z). The distances from the target's center to the transmitter and receiver are represented by r_{c1} and r_{c2} respectively. The target is assumed to move linearly in a plane parallel to the $x-y$ plane with an velocity of v. The angle between the direction of the velocity and the baseline is expressed as ϕ. The projection of target's center to the $x-y$ plane when crossing baseline, expressed as $\mathbf{C}$, has bi static distances d_T and d_R.

The moving target forward scattering signal $E(t)$ of large-diffraction-angle SISAR imaging can be expressed as [4]:

$$
\begin{aligned}
E(t) &= Q_{im} \int_{-\infty}^{+\infty} H_{im}(x') \exp\left(\frac{j\gamma_{im} x'^2}{2v^2}\right) \exp\left(\frac{j\gamma_{im} x' t}{v}\right) dx' \\
Q_{im} &= \frac{A \sin\phi \exp\left[jk(r_{c1} + r_{c2})\right]}{j\lambda r_{c1} r_{c2}} \\
\gamma_{im} &= k\left(1/r_{c1} + 1/r_{c2}\right) v^2 \sin^2\phi
\end{aligned} \tag{1}
$$

where Q_{im} contains the Doppler phase shift and reflects impacts of target geometry to echo signal, $k = 2\pi/\lambda$ is the wave number. γ_{im} is a time-varying parameter determined by the target-center slant range, the track angle, and the target velocity. It is noted that γ_{im} is equal to the Doppler variation rate under small-diffraction-angle assumption at the baseline-crossing time. $H_{im}(x')$ is the CPF function related to the target profile and can be obtained by the inverse transforming of $E(t)$:

$$
\begin{aligned}
H_{im}(x') = \int_{-T_s/2}^{T_s/2} \exp\left(-j\frac{\gamma_{im} x'^2}{2v^2}\right) \times \frac{\gamma_{im}}{2\pi v Q_{im}} \times E(t) \\
\times \exp\left(-j\gamma_{im} x' t / v\right) dt
\end{aligned} \tag{2}
$$

where T_s is the observation interval.

When ignoring the phase introduced by the quadratic term of the target height, the CPF of the target is approximated as follows [4]:

$$
\begin{aligned}
H_{im}(x') &= \left|H_{im}(x')\right| \exp\left[j\psi_{im}(x')\right] \\
&\approx h(x') \operatorname{sinc}\left[k\left(\frac{1}{r_{c1}} + \frac{1}{r_{c2}}\right) z_p h(x') / 2\pi\right] \\
&\quad \times \exp\left[jk\left(\frac{1}{r_{c1}} + \frac{1}{r_{c2}}\right) z_p m(x')\right]
\end{aligned} \tag{3}
$$

where $\left|H_{im}(x')\right|$ and $\psi_{im}(x')$ represent the amplitude and phase of the CPF, respectively. According to (3), the target shadow height difference profile $h(x')$ and median profile $m(x')$ can be extracted from the forward scattering signal of the moving target.

3. Dual-frequency motion compensation

The large-diffraction-angle SISAR imaging algorithm given in (2) can be regarded as a coherent accumulation process. In general, the key to coherent accumulation is the coherence of phase. Similar to other coherent imaging approaches, the focus of SISAR imaging on phase is far greater than the concern for amplitude. We can observe that the parameters to be estimated in the integral of (2) are mainly Q_{im} and γ_{im}. In fact, the accuracy requirement for the estimation of the amplitude of Q_{im} is not quite high. And in most cases the parameter γ_{im} can be approximated by its central value $\gamma_0 = k\left(1/d_T + 1/d_R\right) v^2 \sin^2\phi$. With this in mind, the main problem of motion compensation is the estimation of the phase of Q_{im}. In another word, the accurate Doppler phase history is needed.

According to the electromagnetic theory, the target's forward scattering signal can be written in the form:

$$
E = A_0 \times \frac{1}{r_{c1} r_{c2}} \times \exp\left[jk\left(r_{c1} + r_{c2}\right)\right] \times \dot{\sigma}_s \tag{4}
$$

where A_0 is a complex constant determined by system parameters, $\dot{\sigma}_s$ is the target's complex scattering coefficient. By comparison of (1) and (4), we can express $\dot{\sigma}_s$ as the form of inverse Fourier transform under the assumption $\gamma_{im} \approx \gamma_0$:

$$
\begin{aligned}
\dot{\sigma}_s(t) &= \frac{1}{2\pi} \int_{-\infty}^{\infty} F(x') \exp\left(j\gamma_0 x' t / v\right) dx' \\
F(x') &= \frac{2\pi \sin\phi}{j\lambda} H_{im}(x') \exp\left(j\frac{\gamma_0 x'^2}{2v^2}\right)
\end{aligned} \tag{5}
$$

Further, the time-varying CPF $H_{im}(x')$ is replaced with the time-invariant $H(x')$, the far-field approximate expression of which is:

$$
\begin{aligned}
H(x') &\approx \exp\left[j\frac{2\pi z_p m(x')}{r_F^2}\right] h(x') \operatorname{sinc}\left[\frac{z_p h(x')}{r_F^2}\right] \\
&\approx h(x')
\end{aligned} \tag{6}
$$

Also, under far-field conditions the phase term $\exp\left(j\gamma_0 x'^2 / 2v^2\right)$ can be seen as 1. Then (5) can be rewritten as:

$$
\begin{aligned}
\sigma_s(t) &\approx \frac{1}{2\pi} \int_{-\infty}^{\infty} h(x') \exp\left(j\gamma_0 x' t / v\right) dx' \\
&= \frac{1}{2\pi} \int_{-\infty}^{\infty} h(x') \exp\left[\left(\frac{1}{d_T} + \frac{1}{d_R}\right) v \sin^2\phi\, x' \times kt\right] dx'
\end{aligned} \tag{7}
$$

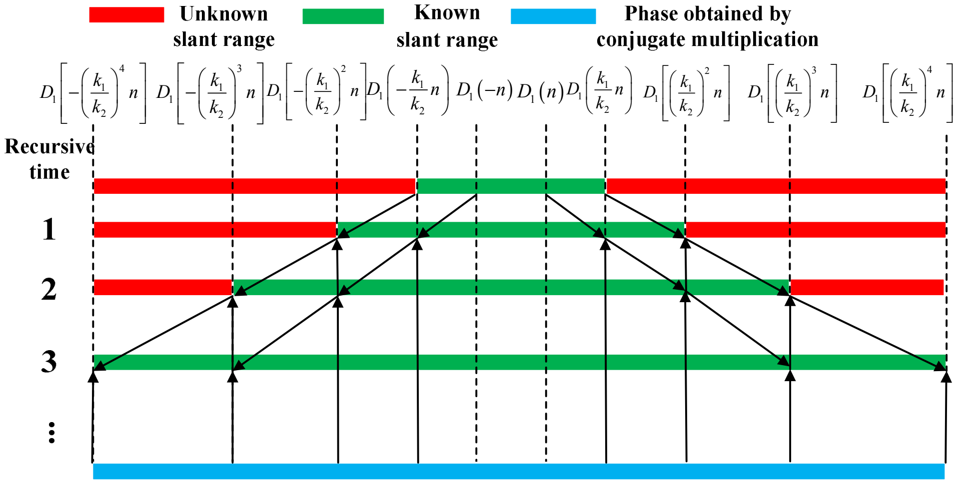

Figure 2. Illustration for the recursive solution of system of equations.

Equation (7) indicates that under the given approximate conditions, there are certain time-scale transformation relations between the target complex scattering coefficients of different wavelengths:

$$\sigma_s(t)_{k_1} = \sigma_s\left[(k_1/k_2)t\right]_{k_2} \tag{8}$$

Next we will show how the above scale transformation relationship can be used for motion compensation. Firstly, the signals of the two carrier frequencies are respectively resampled at sampling rates f_{s1}, f_{s2} and the sampling rates satisfy $f_{s1}/f_{s2} = k_1/k_2$. Then, observation durations of the two signals are set as T_{s1}, T_{s2}, and $T_{s1}/T_{s2} = k_2/k_1$. So the sample points of the two signals are equal and we have:

$$\exp\left[j\varphi_\sigma^{k_1}(n)\right] = \exp\left[j\varphi_\sigma^{k_2}(n)\right] \tag{9}$$

where $n = -N/2, \cdots, 0, \cdots, N/2-1$ denotes the sampling numbers. In another word, the phases of the scattering coefficients of the same sampling point on these two signals are the same.

Using the wavelength-time scale transformation of the complex scattering coefficient, we can compensate the effect of the complex scattering coefficient by using the echo signals of the two frequencies and obtain the accurate estimation of Doppler phase shift from the echo phase. According to (9), phase terms of two signals of the same target can be expressed as:

$$\begin{aligned}\Phi_1(n) &= \exp\left[j\varphi_\sigma^{k_1}(n)\right]\cdot\exp\left[jk_1D_1(n)\right]\\ \Phi_2(n) &= \exp\left[j\varphi_\sigma^{k_2}(n)\right]\cdot\exp\left[jk_2D_2(n)\right]\end{aligned} \tag{10}$$

From the sampling rate relationship we know that $D_2(n) \approx D_1\left[(k_1/k_2)n\right]$. With this in mind, we can carry out the conjugate multiplication the two signals to eliminate the influence of the target scattering phase and obtain the relationship between the conjugate phase and the target-center slant range:

$$\begin{aligned}\Phi(n) &= \Phi_1(n)\cdot\left[\Phi_2(n)\right]^*\\ &= \exp\left[jk_1D_1(n) - jk_2D_2(n)\right]\\ &= \exp\left\{jk_1D_1(n) - jk_2D_1\left[(k_1/k_2)n\right]\right\}\end{aligned} \tag{11}$$

Here we can give an equation set about the estimator $D_1(n)$, where $\Phi(n)$ is the observation, and k_1 and k_2 are the known parameters. In fact, the equation set given in (11) is not easy to solve because each independent equation contains the two slant ranges at sampling point n and $(k_1/k_2)n$. Supposing $k_1 > k_2$, if we have known the $D_1(n)$ which is closer to the baseline-crossing time, we can substitute it into (11) to find $D_1((k_1/k_2)n)$ that is further away from the baseline-crossing time. If follow this recursive mode to continue computing, we can find $D_1(n)$, $D_1\left[(k_1/k_2)n\right]$, $D_1\left[(k_1/k_2)^2 n\right]$, $D_1\left[(k_1/k_2)^3 n\right], \cdots$, as shown in Fig. 2.

So far, the remaining problem is how to find the slope ranges near the baseline-crossing time as the initial value to solve the equation set. Fortunately, the Doppler phase of a target can be expressed as a quadratic term with respect to time using a Fresnel diffraction approximation when the target is approaching the baseline, i.e. when the diffraction angle is small we have:

$$\begin{aligned}&\exp\left[jkD(t)\right] \approx \exp\left(j\frac{\gamma_0}{2}t^2 + j\phi_0\right)\\ &\phi_0 = 2\pi L/\lambda + \pi z_p^2\left(d_T + d_R\right)/\left(\lambda d_T d_R\right)\end{aligned} \tag{12}$$

Although the approximate accuracy of (12) decreases with increasing target-to-baseline distance, the approximate accuracy is quite high for a period of time near the baseline. Therefore, we can use (12) to approximate the target slope distance near the baseline by estimating the Doppler variation rate at the baseline-crossing time. Ignoring the effect of target height, the process of extracting the target slant range by (12) is expressed as:

$$D(t) \approx \frac{1}{k}\left(\frac{\gamma_0}{2}t^2 + \phi_0\right) \tag{13}$$

4. Simulation results

In this section, the proposed method is validated by simulation. The simulation target is a small aircraft model. The silhouette of the model is shown in Fig. 3. The specific simulation parameters are given in Table 1.

Table 1. Simulation parameters

Parameter	Value	Parameter	Value
Baseline	10km	Target height	100m
Track angle	90°	d_T	5km
Wavelength-1	0.6m	Wavelength-2	0.3m
f_{s1}	238Hz	f_{s2}	476Hz
Velocity	100m/s	Target size	4m

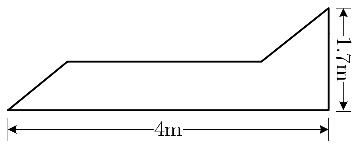

Figure 3. Aircraft model for simulation.

First, the phase error introduced by the approximation in the dual-frequency scale transformation is given, as shown in Fig. 4. When the sampling time for the wavelength of 0.6m is ± 20s (corresponding to azimuth angle ~ ±20 degree), the phase error, or the difference between the scattering coefficient phases of the two resampled signals, is less than 90 degree. Therefore, the maximum time for extrapolating the equation should be less than ± 20s.

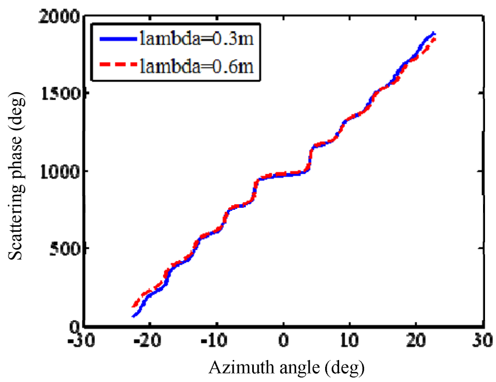

Figure 4. Comparison of dual-frequency scattering phases.

Fig. 5 shows the simulated SISAR images obtained using difference methods: the black lines denotes the real profiles, the blue lines denotes the profiles obtained by ideal large-diffraction-angle SISAR, the green lines denotes the profiles obtained by ideal small-diffraction-angle SISAR, and the red lines denotes the profiles obtained by our method. Here the small-diffraction-angle SISAR used the signal with a Fresnel approximation phase error less than 90 degree, which means the corresponding accumulation time is about ± 5.1s and the resolution is 1.46m. In contrast, the resolution of dual-frequency large-diffraction-angle SISAR imaging with an accumulation time of 16s is 0.47m. We can see that the height difference profile obtained by our method is almost identical to the result of ideal motion compensation. Since the phase is more sensitive to errors, there was some distortion in the median line profile.

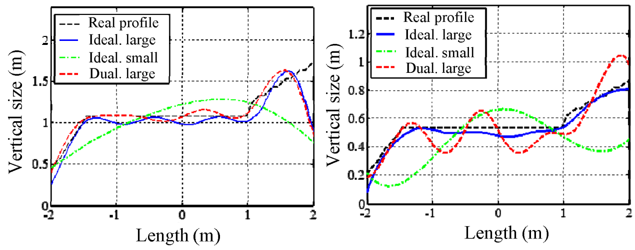

(a)Height difference profiles (b) Median line profiles

Figure 5. Comparison of simulated SISAR images.

5. Conclusions

Overall, the dual-frequency SISAR compensation technique greatly improves the engineering achievable resolution of SISAR imaging. Also its motion compensation can be applied to some unsteady state of motion without the aid of specific model assumptions, which also reflects the robustness of this method.

6. Acknowledgements

This work is supported by the National Natural Science Foundation of China under Grant 317279002.

7. References

1. M. Cherniakov, "Bistatic Radar: Principles and Practice," John Wiley&Sons, 2007.'

2. V. V. Chapurskiy, and V. N. Sablin, "SISAR: Shadow Inverse Synthetic Aperture Radiolocation," The Record of the IEEE 2000 International Radar Conference, Xandria, VA, USA, May 2000, pp. 322-328.

3. C. Hu, C. Zhou, T. Zeng, and T. Long, "Radio Holography Signal Reconstruction and Shadow Inverse Synthetic Aperture Radar Imaging in Ground-based Forward Scatter Radar: Theory and Experimental Results," *IET Radar Sonar & Navig.*, 8, 8, August 2014, pp. 907-916, doi: 10.1049/iet-rsn.2013.0267.

4. T. Zeng, X. Li, C. Hu, and T. Long, "Investigation on Accurate Signal Modelling and Imaging of the Moving Target in Ground-based Forward Scatter Radar", *IET Radar Sonar & Navig.*, 5, 8, August 2011, pp. 826-870, doi: 10.1049/iet-rsn.2010.0276